Brodogradnja Volume 75, Number 2 (2024) 75206

journal homepage: www.brodogradnja.fsb.hr

Brodogradnja

An International Journal of Naval Architecture and Ocean Engineering for Research and Development

Coupled response analysis of dual lifting vessels during collaborative lifting topside module

*Dejiang Li[1,3], Qiutong Tan[*2], Jiwei Liu[2], Long Zheng[3], Chao Hu[4]*

[1] *CIMC Offshore Co., Ltd, Shenzhen, 518000, PR China*
[2] *School of Ocean Engineering and Technology, Sun Yat-sen University, Guangzhou, 518000, PR China*
[3] *Yantai CIMC Raffles Offshore Ltd., Yantai, 264000, PR China*
[4] *College of Shipbuilding Engineering, Harbin Engineering University, Harbin, 150001, PR China*

ARTICLE INFO

Editor-in-Chief: Prof. Nastia Degiuli
Associate Editor: PhD Ivana Martić

Keywords:
Multi-body system
Hydrodynamic response
Interaction
Lifting vessel
Collaborative lifting operations

ABSTRACT

Offshore assembly and disassembly operations represent a multi-billion-dollar market potential. Collaborative lifting by multiple vessels has emerged as a new operating paradigm for integrated offshore facilities assembly and disassembly. Hence, this paper investigates the hydro-dynamic interaction of dual lifting vessels in collaborative lifting operations. The coupled motions during multi-body operations are simulated using the commercial software SESAM. The feasibility of the numerical model for coupled motions in collaborative lifting is verified by comparing the numerical results of topside motions, vessel motions, and vertical lifting arm loads against experimental measurements. The effects of wave heading and period on the hydrodynamic responses of the topside module, dual lifting vessels, and lifting arms during collaborative operations are studied. Their influence patterns and mechanisms are analysed in detail. The results show that transverse waves and head wave induce significant heave and pitch motions of the topside module and vessels, but the maximum vertical loads on the lifting arms occur in oblique waves. The motion responses of the topside module and vessels increase with longer wave periods under the oblique sea condition, and roll motions are more sensitive to large periods compared to the gradual rise in heave and pitch.

1. Introduction

Approximately 1000 oil and gas drilling and production platforms globally weighing over 4000 metric tons are in need of dismantling each year, with demand expected to reach 35-50 platforms annually. Over 300 new offshore platforms are installed worldwide each year [1], demonstrating the substantial market potential for platform installation and dismantling projects valued in the tens of billions of dollars. While established lifting and removal techniques exist for smaller offshore oil-field facilities, large-scale, deep-water platform infrastructure continues to present technical and equipment challenges. As marine systems trend toward increased scale and integration, collaboration operations utilizing multiple heavy lift vessels

[*] Corresponding author.
E-mail address: tanqt@mail2.sysu.edu.cn

http://dx.doi.org/10.21278/brod75206
Submitted 07.12.2023; Accepted 07.02.2024.
ISSN 0007-215X; eISSN 1845-5859

with large pay-loads and coordinated modern control capabilities have emerged as a novel approach for the consolidated installation and dismantling of offshore oil and gas infrastructure.

The mechanical properties of multi-body vessel systems composed of multiple working ships differ significantly from conventional single ship transport and isolated marine equipment. Such collaboration operations fall under the purview of multi-body dynamics in offshore working environments. Since the 1960s, numerous methods for multibody dynamics have been developed, including Huston's vector formulations [2], Roberson-Wittenburg representations[3], Newton-Euler equations of motion [4], Lagrangian mechanics [5] and Kane's method [6], among others. With advances in marine resource utilization, ocean engineering structures have proliferated in number and complexity. In the 1990s, many scholars began exploring the use of multibody dynamics theory to explain the coupling behaviour between substructures of complex marine systems. Dual barge float-over technology is a typical coupled system. In recent year, Dessi et al. [7] experimentally examined double-hull floating transport, simplifying upper structures via modal equivalencing. Elastic versus rigid connection comparisons revealed significant rolling and pitching with elastic block deformations considered. Li [8] simulated the vessel motions in the time domain by using Cummins' approach, emphasizing the gap and its impact on various hydrodynamic results. Ridho Hantoro et al. [9] conducted the numerical simulation and experimental analysis to obtain the relation between the motion response of the pontoon array and its pendulum. Chen et al. [10] investigated the coupled hydrodynamic–structural responses using a frequency–time-domain numerical model with viscous correction [11], in which the mass and stiffness attributes of connectors are incorporated into the system. Liang et al. [12] investigated the free-surface response near resonance in a narrow gap between two fixed, identical barges with square corners numerically and experimentally. Shima et al. [13] used the boundary element method for coupled time-domain dynamic analyses to examine the hydrodynamic interactions between a turret-moored FPSO and shuttle tanker. Ren and Tao [14] investigated the dynamic responses of a two platforms system containing a Tension Leg Platform (TLP) and a tender assisted drilling (TAD) with a flexible connection between the two platforms. The study is revealed that the motion responses for the two platforms in coupled model are altered by the combined effects of the platforms' interaction and constrain by the connection. The coupling effect of DP system is also considered[15,16]. Zhao et al. [17] analyzed the hydrodynamic interactions using a frequency-domain approach, and the effects of the equipped motion compensation equipment and resonant fluids on multibody motions and contact forces based on time-domain simulations are investigated. Chen et al. [18] established a time-domain model, considering various types of mechanical coupling components in the float-over system based on the corrected frequency-domain results. Ji et al. [19] conducted model scale experiments to establish an advanced mathematical model and compared with the quasi-static assumption results. The result shows significant improvements in the motion prediction under DP mode, and a more accurate motion prediction model is successfully established. Zou et al. [20] presented a time domain model that combines the damping lid method and state-space model, resulting in a Constant Parameter Time Domain Model (CPTDM). The finding shows that the damping lid method helps to stabilize the numerical simulation of the multi-body system which undergoes gap resonances. With the application of the motion compensation equipment, the system becomes flexibly connected so that the dynamic behaviors of the novel multibody system become complex. There will be more motion modes of the system, and the effect of couple system responses is uncertain. Parametric studies can be conducted to understand the effects of key design parameters like environmental conditions, crane configuration, and vessel motion on hydrodynamic loads and responses. This supports optimal design of lifting systems. In general, ocean engineering multibody analyses focused on multiple floating bodies and connection assumptions, with limited consideration of topside module motion characteristics during multi-vessel operations.

Cranes can lift payloads of tens of thousands of tons, yet abrupt changes in conditions such as starting, braking, and other operations induce strong vibrations in mechanical systems and dynamic responses in lifting assemblies. Meanwhile, sea states exhibit variability and complexity. During lifting ship operations, the crane moves with the hull, exacerbating swing of lifted objects, reducing positioning efficiency, and potentially threatening safety. Clearly, coupling between lifting and hull motions cannot be ignored. To address these issues, Ren et al. [21] conducted lifting object simulation experiments using MATLAB,

revealing maximal swing angles when excitation and system frequencies coincided. Yang [22] developed a dynamic crane model to study the influence of lifting systems on arm load and object swing load under different conditions, laying foundations for dynamic simulation analysis. Wang et al. [23] studied wave-induced motion responses of crane ship lifting systems, constructing dynamic moored positioning models. Analyses showed external excitation frequencies resembling lifted object characteristic frequencies. When hull motion is simple harmonic, the stable trajectory of the lifting system exhibits many cases depending on hull motion amplitude. During non-harmonic hull motions, the lifting system shakes greatly. Zou Yang [24] used a large semi-submersible floating crane model, calculating significant crane swing amplitudes when natural frequency approached hull motion frequency, indicating frequency proximity strongly influences crane swing. Lin [25] treated the hull as an excitation platform to study lifting system dynamic response during rolling and pitching under regular waves. Calculations showed maximum system response at excitation frequencies equalling natural frequencies. Li et al. [26] establishing an accurate and efficient numerical model to compute the coupled dynamic response between crane SEMISUB and alongside tension leg platform. Lu [27] initially studied motion response characteristics of large crane ship coupled systems via model testing. Resonance occurred under head seas when wave periods neared inherent lifting object periods. Under beam seas, two lifting object motion peaks manifested near rolling periods of both ship and lifting object. Milana et al. [28] carried out dynamic transient analysis of the effects of a payload-carrying trolley moving along the boom using an equivalent planar finite element model. Bozkurt and Melek [29] proposed an efficient solution by integrating the combined vertical, horizontal, and anti-swing control system, experimentally validated mathematical hydraulic system and ship motions on irregular waves, the dynamic model of the crane, and an innovative control strategy. Sun et al. [30] proposed a Multi-Cable Anti-Swing System (MCAS) in terms of a 45-ton crane of a 27,000-ton multipurpose vessel of COSCO Shipping Group as a design prototype, and it is adopted to investigate the dynamic characteristics of the MCAS for cranes within an offshore environment. Makarov et al. [31] investigated the parametric sensitivity of a reduced-scale crane ship numerical model. Masaaki Sano [32] considered a tentative control method to simulate the cooperative manoeuvres under some unique scenarios. Together, these studies emphasize how hull-lifting system coupling dynamics, influenced by frequency relationships and sea conditions, govern offshore lifting operations and safety. Further mathematical modelling and experiments can provide optimization guidelines.

The twin-barge lifting method differs from the traditional float-over deck installation method in the following keyways: In the float-over method, the deck section is floated into position and then slowly lowered onto supporting structures. In the twin-barge lifting method, the deck section is lifted directly into place between two barges, without needing to float it over. With float-over, the deck section must be precisely positioned and lowered into contact with the supporting structures. The twin-barge lifting method allows for more flexibility in positioning as the deck section is lifted rather than floated into place. The float-over method requires the deck section to be buoyant enough to float, which limits the size and weight of deck sections that can be installed. The twin-barge lifting method uses the barges to support the full weight of the deck section during lifting and installation, allowing for larger/heavier deck sections to be installed. Positioning and stability are greater challenges with float-over due to waves and currents that can impact the floating deck section. The twin-barge lifting method provides a more stable and controllable installation process by lifting rather than floating the deck section into place.

Real ship designs and constructions adhere to specific industry standards and specifications [33, 34] The target system under study is an integrated installation and dismantling equipment for collaboration operation of ultra-large offshore oil and gas infrastructure composed of a novel multi-functional lifting vessel. Individual work ships feature multi-body floating bases, while collaboration work introduces complex near-field coupling boundary conditions between multiple bodies. Modern control technologies are also incorporated for collaborative operations, including dynamic positioning, motion compensation, and ballast control, closely linked to fluid-solid coupling. However, practical problems remain in feeding back structural kinematics, dynamic characteristics, and hydrodynamic coupling mechanisms of floating base systems under complex working environments and conditions, especially for collaboration multi-vessel operations. While single vessel analyses provide insights, further research is still needed to fully understand

offshore lifting dynamics involving integrated systems of multiple interacting floating structures. Such studies could help optimize future crane vessel and topside module designs for safe and efficient heavy lift tasks.

This paper investigates the motion characteristics of a topside module and lifting vessels during collaboration dual-vessel heavy lifting operations, using experimental and numerical simulation methods. A coupled numerical simulation model is applied to analyze the module motion, hull motion, and vertical load characteristics of lifting arms under varying wave directions and periods, via the commercial software SESAM. The influence of wave direction and period on the hydrodynamic coupling of the dual-vessel collaboration operation system is explored. Findings provide key design insights for optimizing dual-vessel collaborative heavy lift operations by elucidating how wave conditions impact system dynamics and loads through vessel-vessel and vessel-payload interactions. The results seek to advance safe and efficient offshore module transport and installation via collaboration lifting approaches with multiple heavy lift vessels.

2. Governing Equation

2.1 Wave load

Marine structures are usually subjected to wave loads, wind loads and current loads, which are different from the response in still water. At this time, the dynamic response of floating structures is more complicated. Wave load analysis is the basis and key of structural evaluation and optimization, and it is an important incentive factor for multi-body motion.

The expressions of first-order and second-order wave excitation forces in time domain analysis are as follows：

$$F_w^1(t) = \frac{1}{2\pi}\int_{-\infty}^{t} h_1(\tau)\eta(t-\tau)d\tau \tag{1}$$

$$F_w^2(t) = \left(\frac{1}{2\pi}\right)^2 \int_0^t \int_0^t h_2(\tau_1,\tau_2)\,\eta(t-\tau_1)\eta(t-\tau_2)d\tau_1 d\tau_2 \tag{2}$$

$\eta(\tau)$ is the wave front at time τ, which can be expressed by the linear superposition theory, i.e., the superposition of a series of regular waves with different amplitudes, frequencies and random phases：

$$\eta(\tau) = \sum_{i=1}^{n} \eta_{a_i}\, cos(k_i x - \omega_i t + \varepsilon_i) \tag{3}$$

In the formula, ω_i is the wave frequency of the regular wave, k_i is the wave number, ε_i is the random phase angle and η_{a_i} is the amplitude of the regular wave.

$h_1(t)$ and $h_2(t)$ are the first-order and second-order time-domain wave force coefficients, which can be obtained by Fourier transform with the wave force transfer function $f_w(\omega)$ in frequency domain analysis, as follows：

$$h_1(t) = \frac{1}{2\pi}\int_{-\infty}^{+\infty} f_w^1(\omega) e^{i\omega t} d\omega \tag{4}$$

$$h_2(t_1,t_2) = \frac{1}{4\pi^2}\int_{-\infty}^{+\infty}\int_{-\infty}^{+\infty} f_w^2(\omega_1,\omega_2)\, e^{i(\omega_1 t_1+\omega_2 t_2)} d\omega_1 d\omega_2 \tag{5}$$

According to Eq.(4) and Eq.(5), the time domain wave force coefficient $h(t)$ can be obtained, and then the time history $\eta(\tau)$ of the wave can be obtained according to the wave spectrum, and then the first-order wave excitation force $F_w^1(t)$ and the second-order wave excitation force $F_w^2(t)$ in the time domain analysis can be obtained.

2.2 Wind load

The parameters describing the wind environment conditions mainly include average wind speed, wind speed profile, wind spectrum, etc. In the field of ship and ocean engineering, the average wind speed at a height of 10 m is generally used as a reference. In the specific analysis, there are two ways to consider the wind load: in the stability analysis, the wind load can be considered as a constant load; in the kinematic analysis, it is generally necessary to consider the turbulence effect of wind load.

The wind speed profile describes the change of wind speed with height, which is a coefficient of height:

$$U(z) = U(H)\left(\frac{z}{H}\right)^{\alpha} \tag{6}$$

In the formula, U(z) and U(H) represent the wind speed at the height of z and H respectively, and α is a function of the roughness at the junction of the air layer and the sea surface. It can be considered to be equal to 0.14 in the general case of the sea. For the open sea area with waves, the value of α is 0.11 ~ 0.12.

Due to the need of calculation and analysis, it is often necessary to convert the wind speed to different average periods and reference heights. The specific conversion can refer to the following formula：

$$U(T,z) = U_{10}\left(1 + 0.137 \cdot ln\frac{z}{H} - 0.047 \cdot ln\frac{T}{T_{10}}\right) \tag{7}$$

where T_{10} represents the 10-min average wind speed at 10 m height. For the design and analysis of ocean engineering, the 1-hour average wind speed at 10 m above the sea surface and the time-varying component are generally used to describe the influence of wind on ocean engineering structures in the form of wind spectrum from the perspective of energy.

At present, the wind spectrum widely used in the field of ship and ocean engineering is mainly API spectrum and NPD spectrum. Considering that the wind load gust period of this project is less than 500 s, it is more appropriate to use NPD spectrum to describe the wind environment conditions.

The 1-hour average wind speed $U(z)$ at z meters above sea level can be expressed as：

$$U(z) = U_{10}\left[1 + C\,ln\left(\frac{z}{10}\right)\right] \tag{8}$$

$$C = 0.057\sqrt{1 + 0.15U_{10}} \tag{9}$$

where U_{10} is the one-hour average wind speed at 10 m above sea level.

The NPD spectrum describes the fluctuation of longitudinal wind speed energy density at a certain point, and its expression is：

$$S_{NPD}(f) = \frac{320\left(\frac{U_0}{10}\right)^2\left(\frac{z}{10}\right)^{0.45}}{(1+f^{0.468})^{3.561}} \tag{10}$$

where $S_{NPD}\left(f\right)$ is the energy density of frequency f in $m^2 \cdot s$, f is the frequency in Hz:

$$f_a = \frac{172f\left(\frac{z}{10}\right)^{2/3}}{\left(\frac{U_0}{10}\right)^{3/4}} \tag{11}$$

2.3 Current load

In engineering design, tidal current and ocean current are generally regarded as stable flow. The current load acting on the marine structure can be regarded as a combination of current force and current moment. In the time domain analysis, the drag force generated by the superposition of the current velocity and the horizontal velocity of the wave particle should be considered in the calculation of the current force

and the tidal force, which cannot be calculated separately. The expressions of the flow force and torque are as follows：

$$F_{cx} = 0.5C_{cx}\rho_c v_c^2 T L_{pp} \tag{12}$$

$$F_{cy} = 0.5C_{cy}\rho_c v_c^2 T L_{pp} \tag{13}$$

$$M_{cxy} = 0.5C_{cxy}\rho_c v_c^2 T L_{pp}^2 \tag{14}$$

In the formula, F_{cx} is the longitudinal force, F_{cy} is the transverse force, M_{cxy} is the flow moment around the Z axis, ρ_c is the seawater density, generally 1.025 × 103 kg / m3, v_c is the average flow velocity, T is the average draft of the hull, L_{pp} is the length between the vertical lines of the hull, C_{cx} is the longitudinal flow force coefficient, C_{cy} is the transverse flow force coefficient, and C_{cxy} is the yaw moment coefficient.

2.4 Time domain analysis method

The radiation force of the floating body can be expressed by the following formula:

$$F_j(t) = \mu_{ij}\ddot{x}(t) + \int_{-\infty}^{t} \dot{x}(\tau)\, K_{ji}(t-\tau)d\tau \tag{15}$$

where μ_{ij} is the frequency infinite added mass and K_{ji} is the delay function. They can establish the following relationship with the frequency domain added mass coefficient $m_{ij}(\omega)$ and the damping coefficient $\lambda_{ij}(\omega)$:

$$\mu_{ij} = m_{ij}(\omega) + \frac{1}{\omega}\int_0^{\infty} K_{ij}(t)\, sin\, \omega\, t dt \tag{16}$$

$$K_{ij}(t) = \frac{2}{\pi}\int_0^{\infty} \lambda_{ij}(\omega)\, cos\, \omega\, t d\, \omega \tag{17}$$

The motion equation of the floating structure in the time domain is obtained by transforming the hydrodynamic coefficient characteristics of the floating structure in the frequency domain into the time domain results:

$$\left[M_{ij} + \mu_{ij}\right]\left\{\ddot{x}_j(t) + \int_{-\infty}^{t}\left[K_{ij}(t-\tau)\right]\left\{\dot{x}_j(\tau)\right\}d\tau + C_{ij}x_j(t)\right\} = F_i(t) \tag{18}$$

In the formula, M_{ij} is the mass matrix of the floating structure; μ_{ij} is the additional mass matrix of the structure; $K_{ij}(t-\tau)$ is the time delay function of the structure; C_{ij} is the hydrostatic restoring force coefficient of the structure.

A time-domain coupled numerical simulation model is established within the commercial software environment SESAM [35] to simulate these environmental loadings and fluid-structure interactions during collaboration dual-vessel lifting operations. The model integrates relevant hydrodynamic theory and permits parametric variations to provide insights on system response under changing sea states, assisting in optimization of lifting vessel design and operation.

3. Numerical Model

3.1 Lifting vessel performance parameters

The dual-vessel collaboration lifting operation involves two multi-functional heavy lift vessels primarily using lifting arms to raise the target structure. Fig.1a provides a schematic of the operation configuration. Fig.1b details the numbering scheme for the lifting arms. Fig.1c details the location information. Table 1 lists the key parameters of the multi-purpose lifting vessels used in the two-vessel collaboration operation system. These parameters were incorporated into the numerical model to accurately reflect the vessel characteristics and appropriately capture system dynamics during simulated heavy lift

scenarios. The model setup enables systematic parametric studies by varying factors such as wave conditions, payload location, and vessel separation to deduce optimization guidelines for dual-vessel collaborative lifting operations.

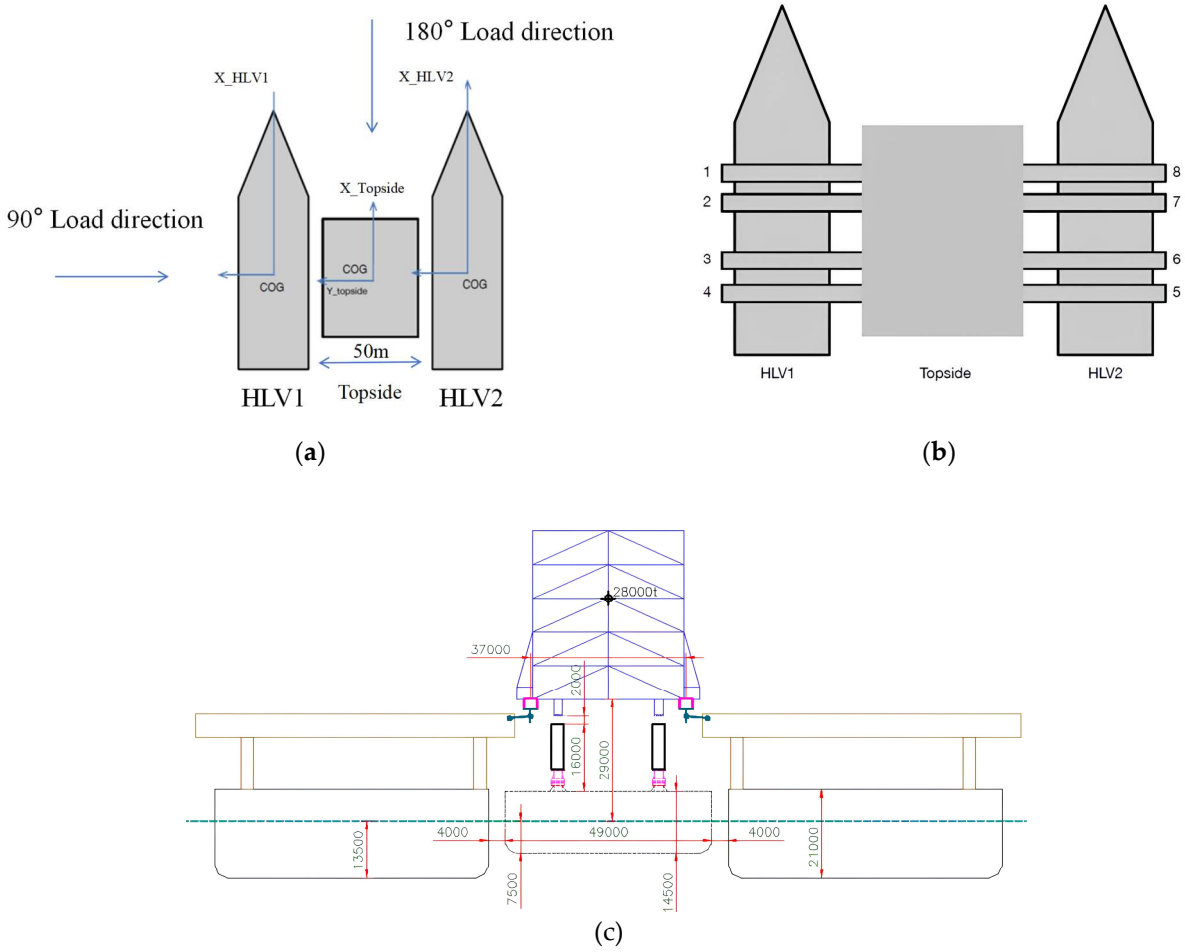

Fig. 1 (a) Collaboration operation position of lifting vessels (left) and (b) Lifting arm number schematic diagram (right).

Table 1 major parameter.

Name	Sign	Unit	Actual value
Length	L_{OA}	m	238
Beam	B		65
Depth	D		44
Depth Moulded to Main Deck	d		21
Center of gravity	G		(111.98，0，24.75)
Height of initial stability	GM		11.83
Displacement	w	t	154500
Rotational inertia around the x shaft	I_{XX}	Kg*m2	5.01E+10
Rotational inertia around the y shaft	I_{YY}		5.27E+11
Rotational inertia around the z shaft	I_{ZZ}		5.19E+11

3.2 Numerical model of multi-body collaborative operation system

To study the hydrodynamic characteristics of the dual lifting vessels, topside module, and vertical lifting arm loads under collaboration lifting operations, a time-domain coupled dynamics simulation model

of the multi-body system was established. The numerical model was designed to realistically represent complex interactions such as multi-body hydrodynamic parameterization, lifting arm simulation, articulation between arms and modules, and dynamic positioning system modelling.

Accordingly, the main components of the multi-body collaboration operation system hydrodynamic analysis model in this work include: 1) A dual-vessel hydrodynamic model of the lifting vessels, 2) Jacket and topside module models, 3) A lifting arm model, and 4) A dynamic positioning system model. Fig. 2a illustrates the complete multi-body hydrodynamic coupling numerical simulation model framework. Together, these model elements capture the essential vessel-vessel, vessel-payload, and environmental loadings to elucidate system dynamics and optimization opportunities for collaborative offshore lifting tasks.

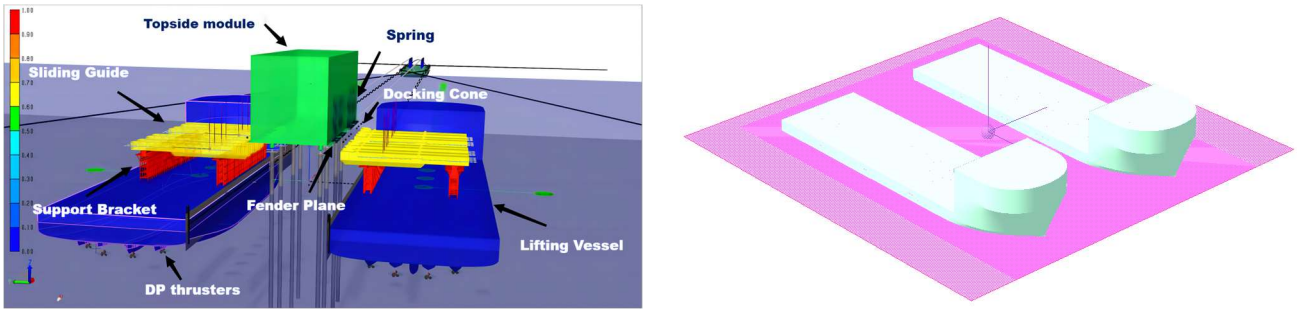

(a) (b)

Fig. 2 (a) The overall schematic diagram of the numerical simulation mode (left) and (b) Two-ship model. (right).

Fig. 2b displays the two multi-functional lifting vessel model established in WADAM. The software was used to compute multi-body hydrodynamic coefficients for the dual crane vessels, which were then imported into the SIMA program. The derived coefficients encompass hydrodynamic interaction parameters between the multiple bodies. In WADAM, rolling viscous damping for individual ships typically considers 3% critical damping. Additionally, at close separation distances between two or more vessels, damping effects due to the intervening free surface must be accounted for. By introducing a free surface mesh model in WADAM and setting a damping coefficient of 0.02, these surface wave damping impacts were incorporated into the numerical model. Proper representation of such hydrodynamic couplings and damping mechanisms between lifting vessels is crucial for accurately simulating offshore module transport dynamics.

Fig. 3a outlines the lifting arm simulation method. Weights are simulated by establishing Fender Planes bearing block loads. Lifting compensation functions are replicated via user-defined stiffness curves. As shown in Fig. 3b, lateral compensation is also simulated. Each arm connects to the ship via four Docking Cones and an intermediate spring. Docking Cones, modelled at 5-10% critical damping, support arm weights while constraining motion to the axial direction. Springs, assigned linear stiffness, provide passive compensation during sliding via prescribed restoring forces. When modelled, arm self-weight application points are positioned consistent with support locations.

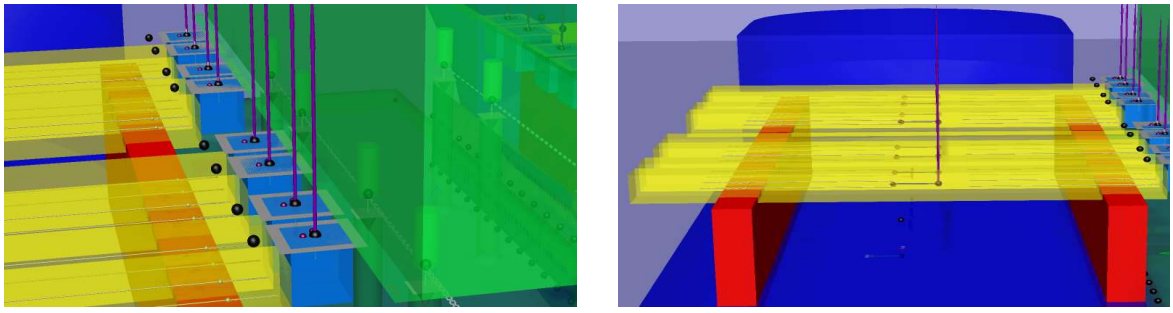

(**a**) (**b**)

Fig. 3 (a) The overall schematic diagram of the numerical simulation mode (left) and (b) Two-ship model. (right).

Fig. 4 illustrates the lifting arm-block connection schematic. Z-direction passive compensation stiffness of the lifting arms is simulated through single-point Fender Planes, which eliminate bending moments at the contact locations consistent with actual design concepts. In contrast, multi-point supports would induce non-representative bending in the model. To prevent block relative sliding along the arms, large stiffness Docking Cone coupling elements are employed to restrict horizontal motion. These Docking Cones mimic the fixed interface between lifting equipment and payload that properly constrains degrees of freedom while enabling vertical compensation behaviour. Together, these connection modelling approaches simulation the load transfer and dynamic interaction behaviours between lifting booms and transported modules.

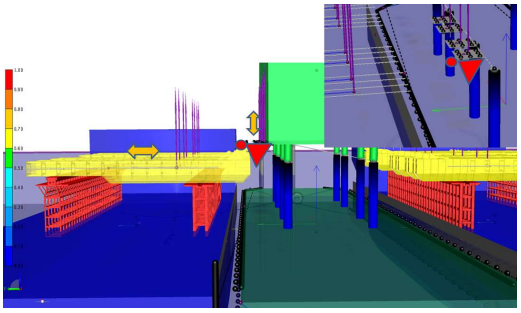

Fig. 4 The schematic diagram of the simulation method of lifting arm and block connection.

Table 2 lists the dynamic positioning (DP) thruster parameters for the lifting vessels, including thruster type, position, power rating, and thrust capability. As depicted in Fig. 5a, the nine thrusters are configured with two tunnel thrusters at the bow, three telescopic thrusters along the main body, and four fully revolving thrusters at the stern. Fig. 5b illustrates the propeller-based thruster modelling approach used. Accurately representing the DP system, comprising thruster characteristics and layout, is imperative for realistically capturing vessel station-keeping and manoeuvring behaviours throughout simulation of the collaborative offshore lifting operations. The numerical modelling of propulsion power and thrust vectors enables investigation of optimal DP-assisted vessel positioning and response to environmental loads.

Table 2 DP Propeller parameters.

Propeller number	Position		Power (kW)	Diameter (m)	Thrust (kN)
	X (m)	*Y* (m)			
1(channel)	108.75	0.0	3000	3.2	429
2(channel)	103.95	0.0	3000	3.2	429
3(extensible)	95.95	0.0	4500	3.9	795
4(extensible)	83.95	0.0	4500	3.9	795
5(extensible)	71.95	0.0	4500	3.9	795
6(full circle)	-104.05	16.8	4500	3.9	781
7(full circle)	-111.25	6.4	4500	3.9	781
8(full circle)	-111.25	-6.4	4500	3.9	781
9(full circle)	-104.05	-16.8	4500	3.9	781

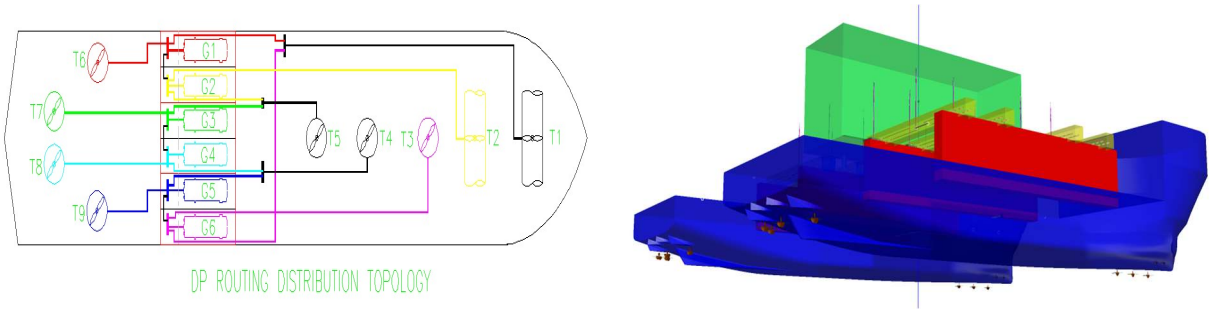

(**a**) (**b**)

Fig. 5 (a) The overall schematic diagram of the numerical simulation mode (left) and (b) Two-ship model. (right).

Within the multi-body collaboration operation system hydrodynamic analysis model, each of the two vessels employs an independent DP control system. Propeller characteristics are parameterized based on practical experience, including setting maximum thrust, maximum thrust rate of change, and maximum rotation angle change rate. Excessive capacity values would induce unrealistic propeller responses. Additionally, the vessels exhibit coupling in rolling and sway motions since relative motions are unconstrained structurally and lifting arms do not experience appreciable bending moments. Therefore, sensitivity to coupling effects must be considered when specifying DP parameters, particularly the DP system period and filter truncation period.

Best practices for specifying DP system periods indicate a relationship greater than 2:1 between overall system period and filter truncation period. Additionally, smaller truncation periods in general provide improved performance but should avoid inducing excessive propeller response to vessel first-order wave motions. Fig. 6 tests sensitivity of truncation period and identifies stable control system periods through analysis of surge, sway, and yaw responses. Fig. 6a plots standard deviation of estimation error versus truncation period. The sensitivity study determines sway, surge, and yaw DP systems remain stable for periods over 115 seconds when utilizing a 40.0 second filter truncation period. Together, these findings inform appropriate DP parameter selection to achieve dynamic station-keeping objectives while plausibly representing propulsion-environment interactions and avoiding unrealistic numerical behaviour during simulation of the complex multi-body collaboration lifting system.

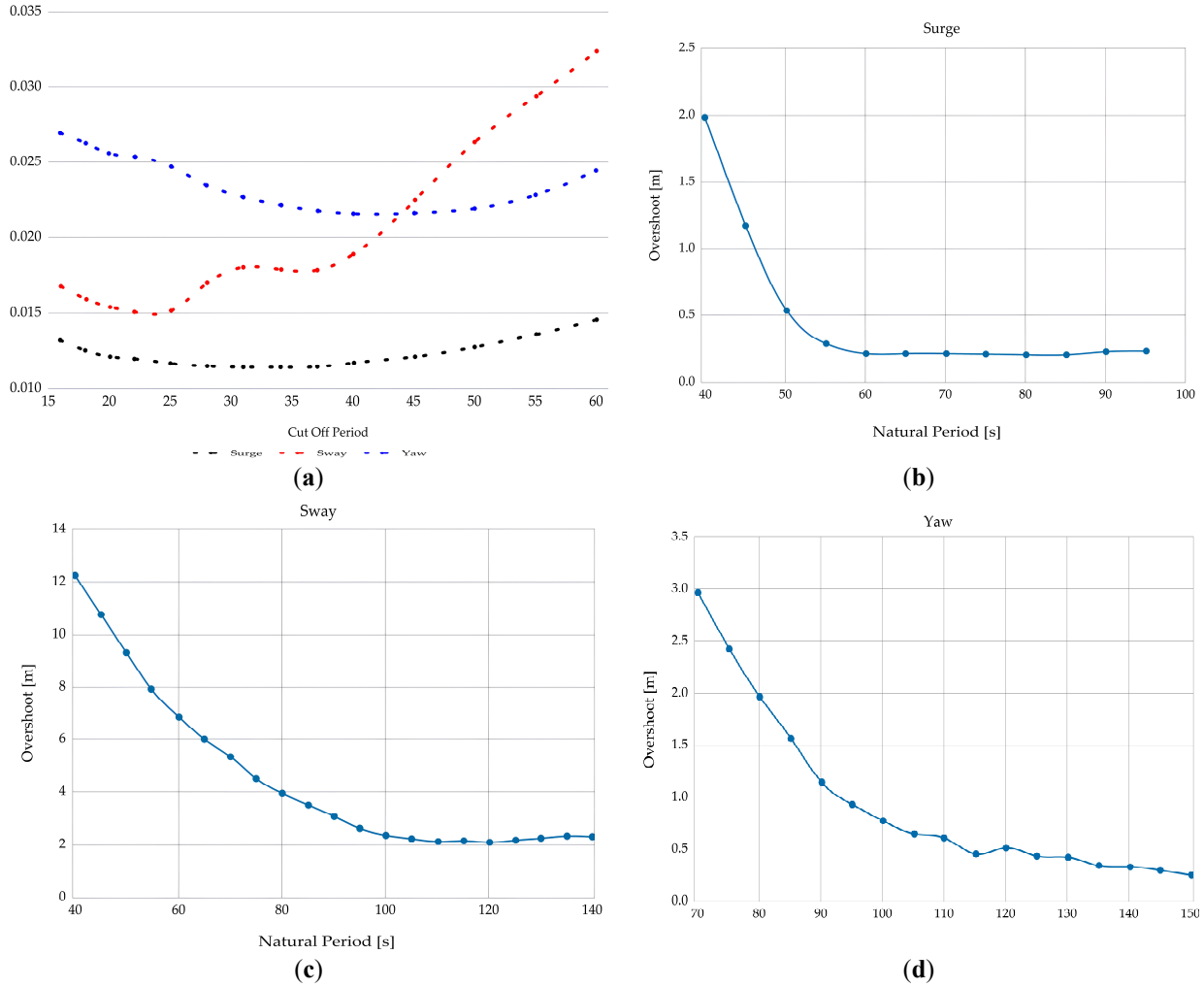

Fig. 6 DP cycle sensitivity test: (a) DP filter truncation cycle sensitivity test; (b) Period sensitivity test of DP surge system; (c) Period sensitivity test of DP swaying system; (d) Period sensitivity test of DP yaw system.

For time-domain simulations of multi-vessel operations, short-term sea conditions spanning 3 hours are typically selected for analyses. CCS GD03-2020 ' Guidelines for Analysis of Transportation and Floatover of Large Offshore Structures 2020 ' Chapter 8 rule 7.8. [36] recommends individual analysis conditions simulate 1-hour durations. Additionally, to reduce sensitivity to random numbers, five random seeds are employed to generate random wave time histories, with statistical response results then averaged to determine final outputs. Considering the large stiffness Docking Cone coupling elements introduced, a small initial time step of 0.005-0.010 seconds is specified to enable numerical convergence, adjusted based on calculated solution behaviour. These modelling parameters balance accuracy needs with computational feasibility requirements for the complex multi-body problem involving close vessel proximity and structural linkage dynamics. The settings allow sufficiently long simulations to capture system response statistics while avoiding potential numerical issues that could obscure meaningful insights into collaboration offshore lifting operations.

3.3 Lifting vessel performance parameters

This paper further analyzes sensitivity to wave direction and wave period to elucidate hydrodynamic characteristics of the multi-body collaboration operation system. Table 3 lists sea state parameters for the wave direction sensitivity analysis, varying wave headings while maintaining a constant spectral significant wave height and peak period. Meanwhile, Table 4 provides specifications for the wave period sensitivity analysis, changing peak periods but holding wave height and direction fixed. Subjecting the multi-body numerical model to variations in these defining sea conditions illuminates system response dependence and hydrodynamic coupling impacts related to environmental forcing. Elucidating such sensitivities equips engineers and operators with insights for designing collaborative lifting tasks and vessels to maintain safety margins under an appropriate scope of representative weather conditions.

Table 3 Sensitivity analysis of wave direction sea state parameters.

Working condition	Significant wave height (m)	Peak period (s)	Wind velocity (m/s)	Flow velocity (m/s)	Loading direction (deg)
A1	1.0	8.0	10	1	90
A2	1.0	8.0	10	1	105
A3	1.0	8.0	10	1	120
A4	1.0	8.0	10	1	135
A5	1.0	8.0	10	1	165
A6	1.0	8.0	10	1	180

Table 4 Sea state parameters of wave period sensitivity analysis.

Working condition	Significant wave height (m)	Peak period (s)	Wind velocity (m/s)	Flow velocity (m/s)	Loading direction (deg)
B1	1.5	8.0	10	1	135
B2	1.5	9.0	10	1	135
B3	1.5	10.0	10	1	135
B4	1.5	11.0	10	1	135
B5	1.5	12.0	10	1	135

4. Model Validation

The numerical simulation results are verified by comparing with model test data for typical operating conditions. A 90° wave direction scenario with 12.0 second peak period is analyzed. Comparisons cover module motion, hull motion, and vertical arm load characteristics. The model test was carried out in the Ocean Engineering Water Tank of Shanghai Jiaotong University. The Ocean Engineering Water Tank can simulate various ocean environment conditions such as wind, wave and current, which is a water tank with comparatively complete technical functions in China. Its main dimensions are 50m×30m×6m. According to

the specified test conditions and the capabilities of test facilities in the basin, the scale ratio of the model test is 1:50. The water depth is adjusted by regulating the position of a large area movable bottom in the basin. The water depth for the model test is proposed as the 2.0m in model scale and 100m in full scale. Table 5 and 6 present the dimension of HLV and topside parameters.

Table 5 Dimension of HLV

Main Dimension	Unit	Full Scale	Model Scale
Length Overall (Hull)	m	238	4.760
Length Between Perpendiculars	m	233.7	4.674
Breadth Moulded	m	65	1.300
Depth Moulded to Main Deck	m	21	0.420
Design Draught (MLD)	m	9	0.180

Table 6 Topside module parameters

Parameters	Symbol	Unit	Full Scale	Model Scale
Length	*L*	m	110.00	2.2
Height	*H*	m	40.00	0.800
Width	*B*	m	36.00	0.72
Weight	*W*	Ton	30000	0.23415
Longitudinal COG	LCG	m	55.00	1.1
Transversal COG	TCG	m	0.00	0
Vertical COG	VCG	m	18.30	0.37
Lifting Support Distance	*D*	m	45.00	0.9
Radius of gyration in Roll (about COG)	*Rxx*	m	17.28	0.3456
Radius of gyration in Pitch (about COG)	*Ryy*	m	34.64	0.6928
Radius of gyration in Yaw (about COG)	*Rzz*	m	33.43	0.6687

In table 7, LAS 1-8 are the lift arm numbers, which can be found in Fig. 1(B). Table 7 presents the Z-direction load of lifting arms comparison for the dual-vessel lifting operation between numerical and physical model results, showing approximately 6% deviation. Fig.7 further illustrates the time-domain response agreement. The close matching load predictions validate the capability of the proposed modelling approach to accurately forecast vertical lifting arm loads, as just a 6% difference falls well within engineering design margins. Overall, verification studies demonstrate the numerical simulations effectively capture essential dynamics of the multi-body collaboration lifting system under representative weather conditions.

Table 7 The comparison results of Z-direction load numerical simulation and model test of lifting arm.

Load contrast		Numerical calculation (N)		Model test (N)		Deviation between numerical calculation and model test	
		Max	Min	Max	Min	Max deviation	Min deviation
Lifting vessel V1	LAS1	4.14E+07	3.19E+07	4.06E+07	3.38E+07	1.98%	-5.67%
	LAS3	3.98E+07	3.33E+07	3.95E+07	3.38E+07	0.74%	-1.39%
	LAS5	3.80E+07	3.51E+07	3.89E+07	3.30E+07	-2.21%	6.24%
	LAS7	3.85E+07	3.50E+07	4.06E+07	3.29E+07	-5.24%	6.33%
Lifting vessel V2	LAS1	4.26E+07	3.17E+07	4.01E+07	3.31E+07	5.99%	-4.34%
	LAS3	4.11E+07	3.32E+07	3.91E+07	3.47E+07	5.05%	-4.10%
	LAS5	3.88E+07	3.49E+07	3.93E+07	3.28E+07	-1.31%	6.35%
	LAS7	3.87E+07	3.53E+07	4.05E+07	3.37E+07	-4.50%	4.71%

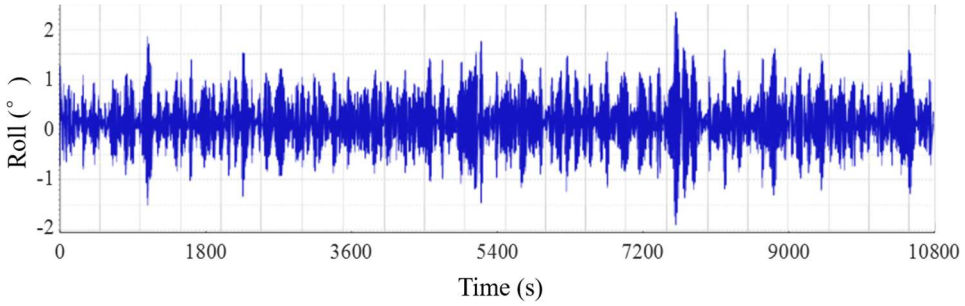

Fig. 7 The Z-direction load time history curve of the lifting arm.

Table 8 The results of numerical simulation and model test motion comparison between the topside module and the lifting vessels are compared.

motion contrast		numerical calculation (N)		model test (N)	
		Max	Min	Max	Min
Topside module	roll (°)	2.353	-1.901	2.353	-2.216
	pitch (°)	0.046	-0.051	0.174	-0.188
	heave (m)	0.570	-0.550	0.729	-0.832
Lifting vessel V1	roll (°)	0.822	-1.000	1.100	-0.999
	pitch (°)	0.100	-0.092	0.166	-0.159
	heave (m)	1.108	-1.113	0.951	-1.017
Lifting vessel V2	roll (°)	1.169	-1.339	1.159	-0.992
	pitch (°)	0.087	-0.085	0.166	-0.159
	heave (m)	1.237	-1.239	1.005	-0.991

Table 8 lists the statistical extremum results from numerical simulation and physical model testing for motion characteristics of the topside module and lifting vessels during dual-vessel collaboration lifting operations under typical sea conditions. Fig.8 further illustrates the time-domain response comparison. From the comparison of numerical simulation and model test results in Table 6, it can be seen that the motion of the topside module and the hull is in a relatively close numerical range, and the motion law is consistent. Since the motion response itself is a small quantity, the percentage of relative deviation between the results of numerical simulation and model test will be relatively large, but the magnitude is basically the same.

Taken together, Tables 7-8 and Figs. 7 demonstrate good agreement between numerical and experimental motion and load outputs. The consistent extremes and following time-variant profiles validate the simulation model's ability to accurately recreate key dynamic behaviours of the complex multi-body system during heavy lifting conditions. Validating motion responses supplements the previous load comparisons, strengthening overall confidence that the numerical model furnishes realistic representations of offshore module transport operations for the given environmental scenario. This validates the simulation model's ability to accurately capture key dynamic behaviours of the complex multi-body system during offshore lifting.

5. Result and Discussion

5.1 Wave direction sensitivity analysis

To further elucidate motion laws and load response characteristics, the established multi-body collaboration operation system hydrodynamic analysis model was used to investigate sensitivity to waves. Motion responses and load behaviours were explored under differing environmental conditions via analysis of single vessel motions and topside module motion simulation. Key parameters included topside module motion amplitude, No. 1 lifting vessel motion amplitude, and LAS4 lifting arm vertical load. Numerical simulations were conducted for six wave directions (90°, 105°, 120°, 135°, 165°, 180°) under 1m significant wave height.

Table 9 provides the maximum, minimum, and range of responses for all six degrees of freedom of the lifting vessel across the wave directions. These sensitivity studies shed light on system dynamics and loadings resulting from variations in sea state parameters like wave heading. Such insight aids optimization of collaborative lifting task planning by characterizing operational thresholds under an appropriate scope of forecasted site conditions. The model thereby supports engineering efforts to enhance operational safety, efficiency and cost effectiveness.

Table 9 Motion response of lifting vessel.

Parameter		90°	105°	120°	135°	165°	180°
Surge (m)	maximum value	0.328	0.593	0.646	0.344	0.322	0.158
	minimum value	0.195	0.302	0.392	0.074	0.100	-0.070
	differentials	0.134	0.291	0.254	0.270	0.222	0.227
Sway (m)	maximum value	0.925	0.722	0.421	0.288	-0.126	-0.350
	minimum value	-0.380	-0.345	-0.293	-0.305	-0.296	-0.453
	differentials	1.305	1.067	0.714	0.593	0.170	0.103
Heave (m)	maximum value	0.273	0.211	0.103	0.059	0.050	0.056
	minimum value	-0.248	-0.201	-0.096	-0.051	-0.050	-0.059
	differentials	0.521	0.411	0.198	0.109	0.100	0.115
Roll (deg)	maximum value	0.461	0.257	0.202	0.172	0.179	0.173
	minimum value	-0.465	-0.238	-0.120	-0.034	0.089	0.126
	differentials	0.926	0.495	0.322	0.206	0.090	0.047
Pitch (deg)	maximum value	0.034	0.269	0.139	0.060	0.158	0.099
	minimum value	-0.033	-0.257	-0.140	-0.062	-0.170	-0.100
	differentials	0.067	0.526	0.279	0.122	0.328	0.199
Yaw (deg)	maximum value	-0.150	-0.248	-0.346	-0.033	-0.174	0.055
	minimum value	-0.301	-0.630	-0.765	-0.410	-0.300	-0.111
	differentials	0.151	0.382	0.419	0.378	0.127	0.167

Table 10 Topside module motion response.

Parameter		90°	105°	120°	135°	165°	180°
Surge (m)	maximum value	0.121	0.142	0.093	0.091	0.110	0.159
	minimum value	-0.096	-0.239	-0.228	-0.181	-0.119	-0.114
	differentials	0.217	0.381	0.322	0.272	0.229	0.273
Sway (m)	maximum value	1.125	1.040	0.812	0.688	0.270	0.053
	minimum value	-0.015	-0.001	0.095	0.093	0.095	-0.047
	differentials	1.140	1.041	0.717	0.594	0.175	0.100
Heave (m)	maximum value	0.281	0.102	0.003	-0.019	-0.043	-0.026
	minimum value	-0.431	-0.247	-0.145	-0.14	-0.155	-0.162
	differentials	0.712	0.349	0.148	0.121	0.112	0.136
Roll (deg)	maximum value	0.557	0.468	0.326	0.242	0.112	0.027
	minimum value	-0.025	-0.016	-0.020	0.002	-0.050	-0.031
	differentials	0.582	0.484	0.346	0.240	0.162	0.058
Pitch (deg)	maximum value	0.036	0.197	0.144	0.075	0.085	0.117
	minimum value	-0.038	-0.220	-0.144	-0.071	-0.085	-0.118
	differentials	0.075	0.417	0.287	0.147	0.170	0.235
Yaw(deg)	maximum value	-0.165	-0.332	-0.449	-0.083	-0.165	0.055
	minimum value	-0.299	-0.547	-0.645	-0.380	-0.300	-0.100
	differentials	0.134	0.215	0.196	0.297	0.135	0.155

Analysis of the lifting vessel response statistics reveals that under identical 1m wave height and period, the multi-body system exhibits larger sway, heave, roll and pitch motions as primary dynamic responses. Comparison of sway and roll variations with direction indicates responses gradually decrease from transverse (90°) to head waves (180°), with wave direction highly sensitive. Swaying waves predominantly influence sway and roll motions, while head seas have little effect. Heave responses decrease from transverse to oblique waves, then increase to head seas, signifying heave effects also warrant attention

in transverse and head conditions. Maximum yaw occurs in oblique 135° waves, gradually decreasing to transverse and head waves - thus requiring consideration in engineering analyses.

Table 10 presents maximum and minimum values of all six degrees of freedom motions for the topside module across the six wave directions, and the ranges.

Analysis of the topside module time histories and statistics reveals its motion responses largely follow trends consistent with the lifting vessel. Block motions couple strongly to those of the vessels. Significant swaying, heaving, rolling and yawing responses are evident. Swaying and rolling mainly depend on transverse waves, while heaving relates to both transverse and head waves. Yawing motions correlate most strongly to oblique waves, especially at 135°.

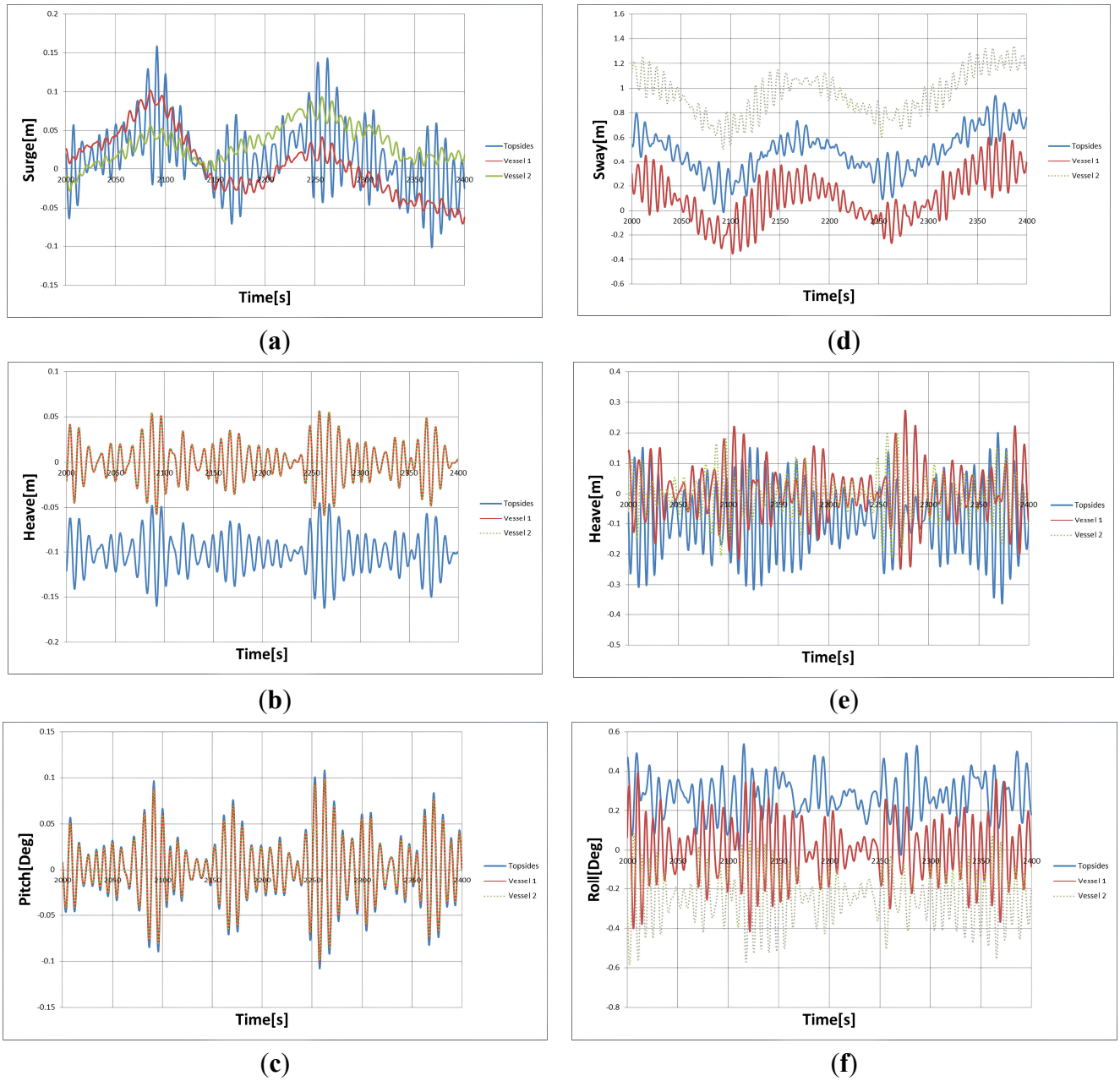

Fig. 8 180 ° wave to the multi-body system motion comparison (a) Surging; (b) Heave; (c) Pitching (left) and 90 ° wave to the multi-body system motion comparison (e) Swaying; (f) Heave; (g) Rolling (right).

To further explore characteristic degree-of-freedom relationships between the topside module and two lifting ships, motion curves under 90° and 180° representative wave directions are compared. In 180° head seas, surge, heave and pitch demonstrate clear responses as depicted in Figs. 8a-c. Surging trends and

periods align between vessels but with different magnitudes, alternating in phase and out of phase between block and ships. Heave and pitch replicate vessel motions identically.

Under 90° transverse waves, prominent responses include sway, heave and roll, shown in Figs. 8e-g. Swaying trends and periods largely correspond between module and vessels over matched periods, while alternating directions reveal complexity. It can be seen that the swaying motion trend and period of the topside module and the two ships are basically similar, and the swaying motion period between the topside module and the two ships is the same, but the motion direction alternates with the same motion direction and the opposite motion direction over time, which also shows the complexity of the multi-body motion system.

Analysis of the multi-body system's rolling motion curves finds the two vessels roll in opposite directions, while the topside module closely follows the motion of Vessel 1. This phenomenon was also observed during physical model testing.

Fig. 9 directly compares the model test and simulation states of the multi-body system subjected to 90° transverse waves. The consistent rolling phasing validates the numerical model's ability to accurately capture this important characteristic dynamic interaction between lifting vessels transporting offshore modules. Namely, the vessels naturally roll against each other to some degree due to wave-induced motions, and the module primarily rolls with the leading vessel.

Such verification reinforces confidence in the model's realism in depicting key behaviours that engineers must understand to appropriately design heavy lift tasks, load transfer systems between vessels and cargo, and vessel positioning considerations. The simulations may therefore provide useful insights into optimization of collaborative offshore lifting operations.

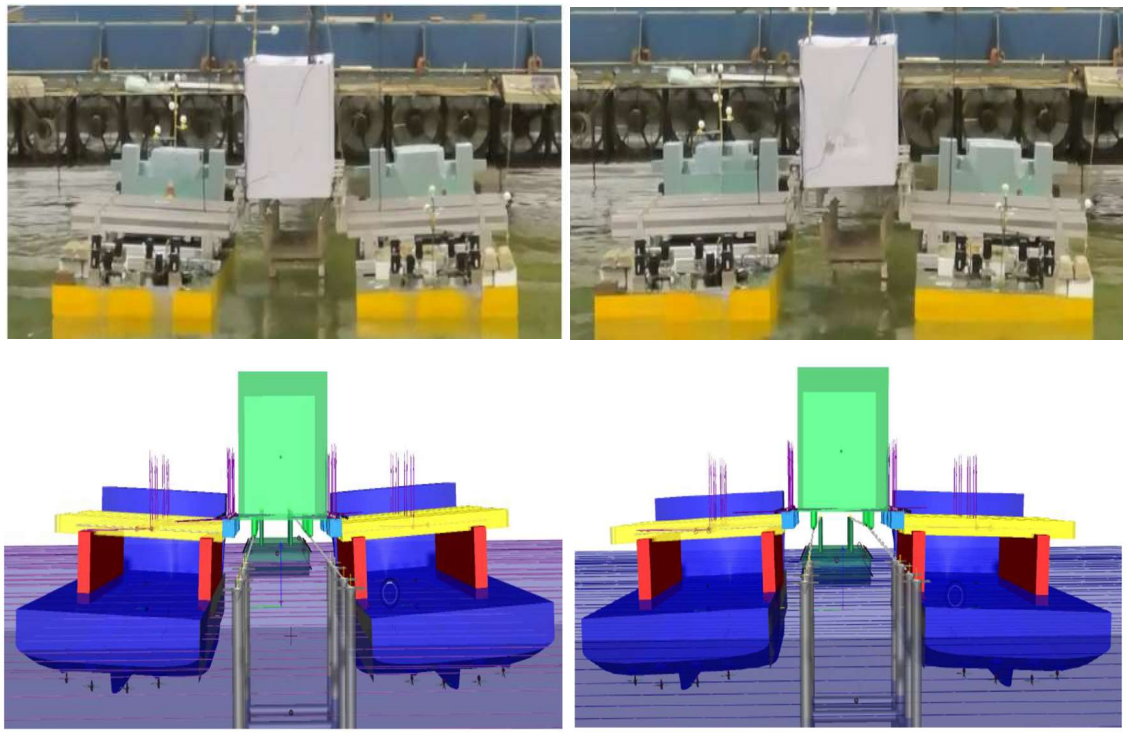

Fig. 9 State comparison between model test and simulation analysis of multibody system

Through the described phenomena and data, it is evident the multi-body system exhibits obvious coupled motions. There is a strong coupling between the rolling of the topside module and lifting vessels, particularly in transverse wave directions. A strong correlation exists between the rolling motion amplitude of the topside module and that of the lifting vessels. Larger rolling amplitudes in the vessels often correspond to larger amplitudes in the module. This underscores the importance of characterizing vessel rolling behaviours and properly accounting for vessel-module interactions driven by environmental loads.

The results enhance understanding of critical load transfer and relative motion effects that define multi-body system performance in offshore module transportation operations.

Fig. 1b illustrates the numbering scheme for the lifting arms. Shown in Fig. 10 is the vertical load time history curve of Lifting Arm No. 4 under a 165° wave condition. To quantify load sensitivity, Table 11 extracts the maximum, minimum, and range of vertical loads exerted on this arm across the six wave directions studied.

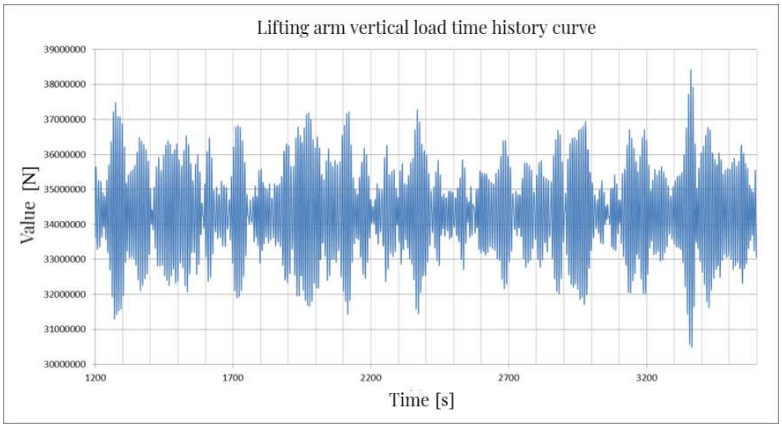

Fig. 10 Time history curve of vertical load of lifting arm under 165° wave action.

Table 11 Vertical load of lifting arm.

Parameter		90°	105°	120°	135°	165°	180°
Vertical load of lifting arm (ton)	maximum value	3655.88	4331.75	3869.82	3829.64	3936.71	3552.48
	minimum value	3311.93	2711.52	3128.99	3165.09	3107.89	3452.14
	mean value	3483.91	3521.64	3499.41	3497.37	3522.3	3502.31
	differentials	343.950	1620.22	740.824	664.54	828.82	100.34

The mean vertical load on the lifting arm remains relatively uniform across wave directions, with small differences. Load variations are smaller for transverse and head waves compared to oblique waves, where larger differences occur. Despite notable heave responses in transverse and head seas, maximum arm loads occur under oblique 105° and 165° waves rather than 90° transverse or 180° head waves. This indicates greater relative motion between the topside module and dual lifting vessels in oblique waves, impacting arm loads more significantly. Therefore, further study of period influences under the 135° oblique wave direction will provide more understanding of load responses and hydrodynamic characteristics of the multi-body system under different environmental conditions.

In summary, comprehensive analyses of vessel and module motions provided valuable insight into how their interactions are affected by environmental loads. The lifting vessel exhibited greater sway, heave, roll and pitch as primary dynamic responses. Module motions closely followed vessel trends, indicating strong coupling. Motions generally decreased from transverse to head waves, with some exceptions like heave. Comparisons of module and vessel motion curves revealed alternating in-phase/out-of-phase surging in head seas and corresponding swaying periods but opposing directions in transverse seas. This demonstrated the complexity of modeling multi-body dynamics accurately. Validation with physical tests further increased confidence in the model. Load sensitivity was also examined, showing vertical loads on the lifting arm varied more for oblique vs transverse/head waves despite notable heave. This implied greater relative motions between module and vessels in oblique seas, highlighting the importance of characterizing such interactions.

5.2 Wave period sensitivity analysis

A 135° oblique wave condition with 1.5m significant wave height is selected as the representative working scenario to conduct wave period sensitivity analysis. Numerical simulations are run for five peak periods - 8, 9, 10, 11, and 12 seconds - to elucidate period influences on the multi-body system.

Fig. 11 shows the heave, roll, and pitch motion time histories of Vessel 1 under 9 and 11 second peak periods. Table 12 then summarizes the maximum, minimum, and ranges of these three motions across all five simulated periods.

Direct comparison of the time-domain responses provides qualitative insight into variations in period, while statistical metrics capture quantitative changes. Such analyses reveal trends aiding characterization of operational thresholds under different forecast conditions. The simulations thus continue supporting optimization of collaborative lifting operations by informing consideration of period impacts on load distributions and dynamic vessel-module interactions defining system performance.

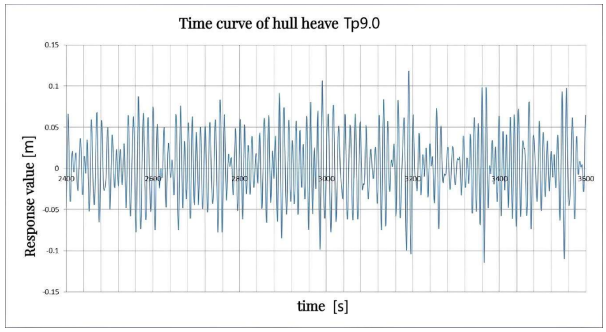

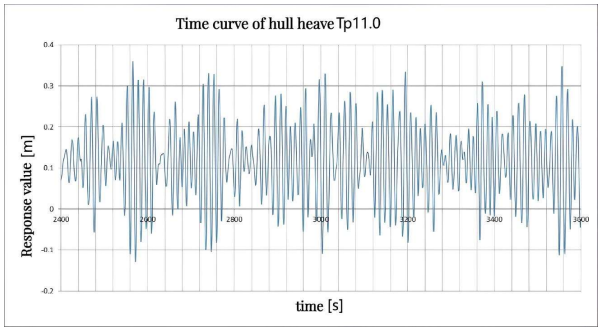

(**a**)

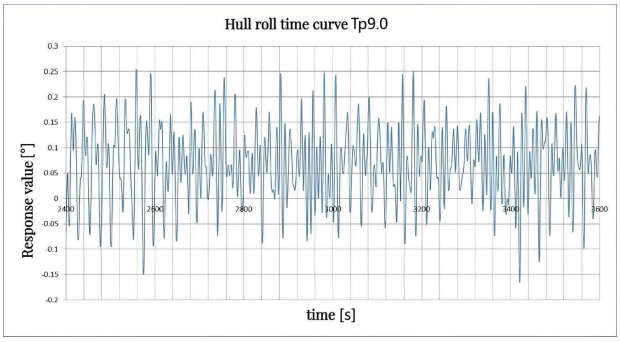

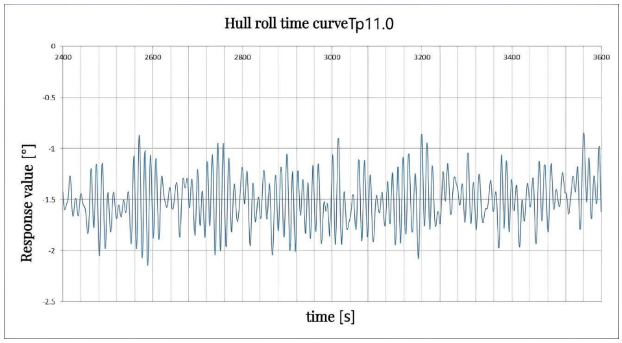

(**b**)

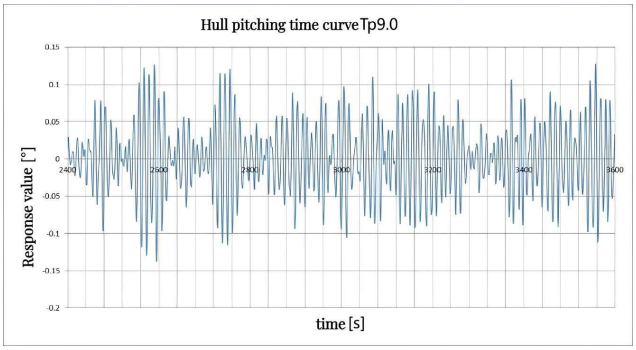

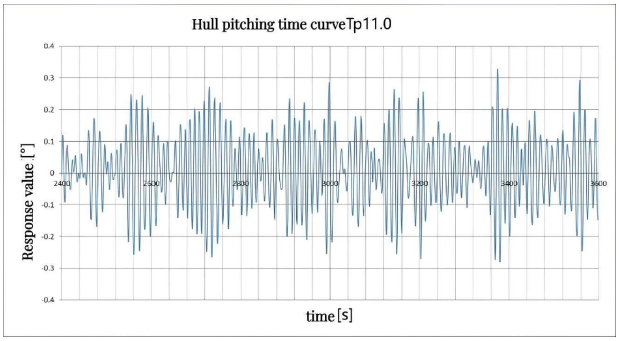

(**c**)

Fig. 11 The lifting vessel motion under the action of wave period 9s and 11s. (a) Heave; (b) Rolling; (c) Pitching.

Table 12 Motion response of lifting vessel.

Parameter		8 s	9 s	10 s	11 s	12 s
Surge (m)	maximum value	0.441	0.465	0.377	0.738	0.850
	minimum value	0.046	0.015	-0.244	0.120	0.270
	differentials	0.395	0.450	0.621	0.618	0.580
Sway (m)	maximum value	0.612	0.488	-0.109	0.011	-0.062
	minimum value	-0.399	-0.415	-1.249	-0.897	-0.828
	differentials	1.011	0.903	1.140	0.908	0.766
Heave (m)	maximum value	0.087	0.122	0.182	0.359	0.450
	minimum value	-0.077	-0.114	-0.165	-0.127	-0.243
	differentials	0.163	0.236	0.347	0.487	0.694
Roll (deg)	maximum value	0.236	0.254	0.514	-0.847	-0.635
	minimum value	-0.116	-0.168	-0.334	-2.143	-2.285
	differentials	0.352	0.422	0.848	1.296	1.650
Pitch (deg)	maximum value	0.084	0.133	0.260	0.331	0.340
	minimum value	-0.082	-0.137	-0.245	-0.290	-0.354
	differentials	0.166	0.270	0.504	0.621	0.694
Yaw (deg)	maximum value	-0.112	-0.004	0.428	0.569	0.215
	minimum value	-0.488	-0.526	-0.601	-0.718	-0.559
	differentials	0.376	0.522	1.028	1.287	0.774

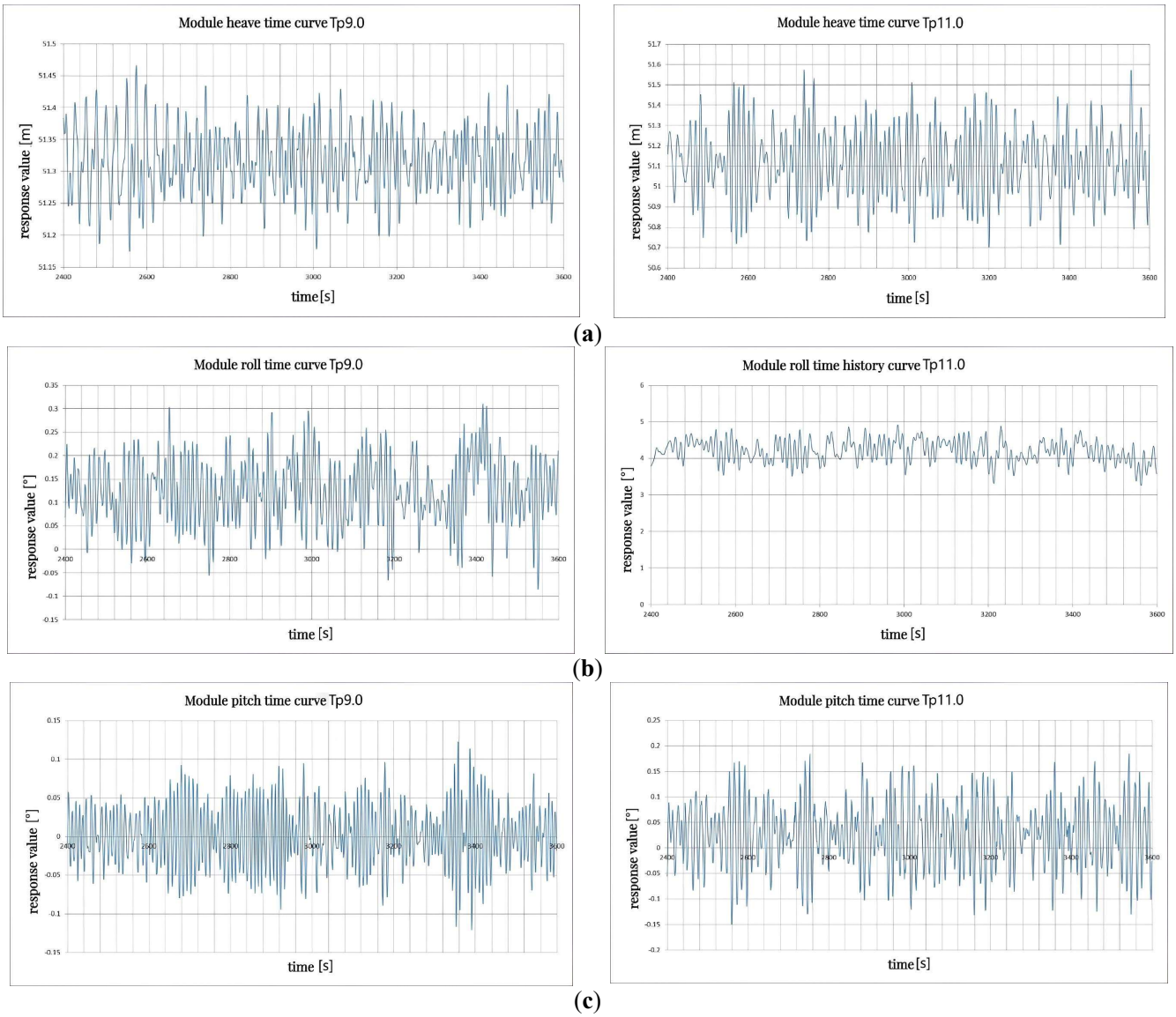

Fig. 12 The motion of the block under the action of wave periods of 9s and 11s (a) Heave; (b) Rolling; (c) Pitching.

Fig. 12 depicts the time-varying response curves for the heave, roll, and pitch degrees of freedom of the topside module under regular waves with periods of 9 seconds and 11 seconds. Table 13 quantitatively summarizes the maximum, maximum and total amplitude range (difference between maximum and minimum) for the heave, roll, and pitch motions.

Table 13 Topside module motion response.

Parameter		8 s	9 s	10 s	11 s	12 s
Surge (m)	maximum value	0.152	0.162	1.305	0.880	0.760
	minimum value	-0.335	-0.283	0.705	-0.160	-0.043
	differentials	0.486	0.445	0.600	1.040	0.803
Sway (m)	maximum value	0.997	0.872	1.066	-0.502	-0.456
	minimum value	0.002	-0.020	-0.073	-1.308	-1.268
	differentials	0.995	0.892	1.139	0.806	0.812
Heave (m)	maximum value	0.012	0.066	0.186	0.178	0.319
	minimum value	-0.178	-0.225	-0.525	-0.707	-0.870
	differentials	0.190	0.291	0.711	0.885	1.189
Roll (deg)	maximum value	0.314	0.310	0.833	4.916	5.227
	minimum value	-0.003	-0.085	-0.337	3.261	3.291
	differentials	0.317	0.395	1.170	1.655	1.936
Pitch (deg)	maximum value	0.112	0.128	0.186	0.184	0.245
	minimum value	-0.105	-0.120	-0.087	-0.150	-0.198
	differentials	0.217	0.248	0.273	0.334	0.443
Yaw(deg)	maximum value	-0.197	-0.158	0.472	0.342	0.162
	minimum value	-0.428	-0.394	-0.805	-0.404	-0.372
	differentials	0.231	0.236	1.277	0.746	0.534

Analysis of the time history curves and motion values in the table reveal that the heave, roll, and pitch response trends of the topside module are consistent with those observed for the lifting vessel alone. All motions increase gradually with rising wave period, as seen for heave and pitch. However, when the incident wave period reaches 11 and 12 seconds, the roll response of the topside module is substantially impacted by the coupled dynamic motion of the connected lifting vessel. At these longer periods, the roll amplitude abruptly augments in a manner that destabilizes the original static equilibrium position. This induces a new oscillating equilibrium state characterized by an increased bounded amplitude range for roll motion. Therefore, when the wave period surpasses a critical threshold, the topside module experiences an abrupt loss of roll stability and change in natural rolling frequency through its hydrodynamic linkage with the lifting vessel. These findings emphasize the importance of considering fully coupled multi-body system dynamics, particularly for rolling response under large period waves, during engineering design and operational planning for combined lifting vessel-topside module systems.

In summary, the wave period sensitivity analysis provides useful insights into how the dynamic behavior of the lifting vessel and topside module system varies with different wave periods. Understanding period impacts is important for operational planning and safety. The finding that both the vessel and module experience an abrupt loss of stability and change in rolling natural period once the wave period surpasses a critical threshold suggests there is a resonant effect occurring between the wave period and the natural rolling frequencies of the bodies. Further dynamic analysis could help characterize this resonance phenomenon more precisely. The nonlinear increase in rolling motions at longer 11-12 second periods indicates potential risks to stability and load control that must be carefully considered for forecast conditions with such swell periods. Operational thresholds may need to account for this sensitivity. The consistency between vessel and module response trends reinforces that a fully coupled dynamic analysis is needed to accurately predict motions, rather than considering the bodies independently. Their interactions play a key role, especially regarding rolling motions. While initial static equilibrium is lost, the system reaches a new oscillating equilibrium state at longer periods. Further study of energy transfers between bodies and degrees-of-freedom could provide insight into this dynamic behavior. Additional environmental conditions like directional spreading should also be examined to better represent realistic sea states and their impacts on the

system. The period-dependent motion responses have implications for load distributions, structural integrity assessments, and operational safety/risk analyses that must be incorporated into system design and planning.

6. Conclusions

A numerical simulation model of multi-body collaboration operation system is established utilizing the commercial software SESAM. Validation of the proposed multi-body system simulation approach was conducted by comparing numerical results under typical operating conditions against experimental data in this paper. The model was employed to further investigate motion behaviors and load responses within the multi-body system through sensitivity studies of wave direction and period during collaboration lifting operations. Specifically, the dynamic responses of both the topside module and dual lifting vessels, as well as the vertical load characteristics on the lifting arms, were examined in detail. The following conclusions are drawn：

(1) The fidelity of the developed multi-body collaboration system numerical model was validated through comparison with physical model test data under representative operating scenarios. By examining key output parameters from both the numerical simulations and experimental model tests, strong accordance between the two approaches was observed. Specifically, the motions of the topside module and vessel hulls from the numerical model fell within a close quantitative range of the experimental measurements. Further, the motion patterns exhibited good qualitative consistency over time. Vertical loads on the lifting arms from the numerical model showed a maximum deviation rate of approximately 6% from experimentally obtained values, indicating small deviation. Together, the close correlation between numerical and physical model results for motion responses and loads verifies the accuracy of the multi-body system numerical simulation framework within an acceptable margin of deviation.

(2) The sensitivity analysis of wave direction revealed that sway, heave, roll and pitch motions of the multi-body system were greatest under oblique waves. Specifically, the transverse wave played a dominant role in inducing sway, roll and heave responses. For heave motion, the topside module and vessel hulls exhibited an in-phase oscillation over time, alternating between moving in the same and opposite directions. The head wave had minimal influence on sway and roll, but did notably impact heave response. Maximum yaw motions occurred under a 135° oblique wave, decreasing for transverse and head waves. These findings demonstrate the importance of considering oblique wave conditions in engineering design.

Heave motions of the topside module and lifting vessels were most evident under transverse and head seas. However, peak vertical loads on the lifting arms occurred under 105 and 165° oblique waves. This suggests relative motions between the modular unit and vessels were heightened under these oblique conditions, translating to greater load impacts on the lifting equipment. In contrast, vertical arm loads remained relatively uniform and stable for transverse and head seas. The sensitivity studies provided valuable insight into how wave direction modulates motion patterns and load distributions within the multi-body system.

(3) The sensitivity analysis revealed that motion responses of the lifting vessel increased non-linearly with growing wave period, consistent with trends observed for the topside module. Both heave and pitch motions rose gradually with period. However, the rolling degree of freedom demonstrated disproportionate amplification at longer periods. Specifically, when the wave period reached 11 and 12 seconds, the amplitude of rolling motion abruptly augmented in a manner that destabilized the original static equilibrium position. This induced a new oscillating equilibrium state characterized by an expanded bounded range for rolling oscillations. This abrupt loss of stability and change in rolling natural period once a critical threshold period was surpassed suggests non-linear dynamics dominate the rolling response under long-period waves. Therefore, the results emphasize the importance of carefully accounting for potentially aggressive rolling behaviors experienced by all components of the multi-body system under large periodic seas. Proper consideration of this non-linear rolling response will be crucial for engineering design and operational safety assessments, given the system's heightened sensitivity in these long-wave conditions.

Overall, the validated multi-body system numerical model proves a useful tool for advancing fundamental understanding of load distributions, motion patterns and hydrodynamic interactions that arise during collaborative heavy lift operations involving dual offshore vessels.

Acknowledgement

This research was funded by the General Project of Guangdong Province Department of Natural Resources to Promote High-quality Economic Development (No.GDOE [2020]026, No.GDOE [2022]30), Shandong Province Major Project (No. 2021CXGCO10701) and National Natural Science Foundation of China (52071348).

REFERENCES

[1] Feng, R. D., Li, Y. D., Ding, B., Sun, T, Li, Y. F., Liu, P., 2020. Analysis of the Adaptability of Offshore Platform Structure Type and Floating Lifting Method. *Ocean Engineering Equipment and Technology*, 7(05), 275-279 (in Chinese).

[2] Huston, R. L., 1981. Multi-Body Dynamics Including the Effects of Flexibility and Compliance. *Computers & Structures*. 14, 443–451. https://doi.org/10.1016/0045-7949(81)90064-X

[3] Liu, J. X., Zhang, W. M., 2007. Automobile Rigid Multi-Body Handling Stability Model and Its Stability Analysis. *Journal of University of Science and Technology Beijing*, 2007(07), 739-743 (in Chinese). https://doi.org/10.13374/j.issn1001-053x.2007.07.020

[4] Truong, V. T., Hwang, Y. L., 2015. Dynamic Analysis and Control of Multi-Body Manufacturing Systems Based on Newton–Euler Formulation. *International Journal of Computational Methods*, 12(02), 1550007. https://doi.org/10.1142/S0219876215500073

[5] Peymani, E., Fossen, T. I., 2015. Path Following of Underwater Robots Using Lagrange Multipliers. *Robotics & Autonomous Systems*, 67, 44–52. https://doi.org/10.1016/j.robot.2014.10.011

[6] Seif, M. S., Inoue, Y., 1998. Dynamic Analysis of Floating Bridges. *Marine Structures*, 11, 29–46. https://doi.org/10.1016/S0951-8339(97)00012-9

[7] Dessi, D., Faiella, E., Saltari, F., Pigna, C., Celli, C., Miliante, T., Di Paolo, E., 2017. Experimental Analysis of the Station Keeping Response of a Double-Barge Float-Over System With an Elastically Scaled Physical Model. *27th International Ocean and Polar Engineering Conference, ISOPE 2017*, 25-30 June, San Francisco, California, USA.

[8] Li, B. B., 2020. Multi-body hydrodynamic resonance and shielding effect of vessels parallel and nonparallel side-by-side. *Ocean Engineering*, 218, 108188. https://doi.org/10.1016/j.oceaneng.2020.108188

[9] Hantoro, R., Septyaningrum, E., Hudaya, Y. R., Utama, I. K. A. P., 2022. Stability analysis for trimaran pontoon array in wave energy converter – pendulum system (WEC - PS). *Brodogradnja*, 73(3), 59–68. https://doi.org/10.21278/brod73304

[10] Chen, M., Ouyang, M., Guo, H., Zou, M., Zhang, C., 2023. A Coupled Hydrodynamic–Structural Model for Flexible Interconnected Multiple Floating Bodies, *Journal of Marine Science and Engineering*, 11(4), 813. https://doi.org/10.3390/jmse11040813

[11] Chen, M., Guo, H., R. R, Wang., N, Tao,. 2021. Cheng, Effects of Gap Resonance on the Hydrodynamics and Dynamics of a Multi-Module Floating System with Narrow Gaps, *Journal of Marine Science and Engineering*, 9(11), 1256. https://doi.org/10.3390/jmse9111256

[12] Liang, H., Chua, K. H., Wang, H. C., Choo, Y. S., 2021 Numerical and experimental investigations into fluid resonance in a gap between two side-by-side vessels, *Applied Ocean Research*, 111, 102581. https://doi.org/10.1016/j.apor.2021.102581

[13] Shima, T., Rouzbeh, S., Rezvan, A., 2021. Numerical investigation on the multi-body hydrodynamic interactions under Caspian Sea environmental conditions. *Ocean Engineering*, 232, 109048. https://doi.org/10.1016/j.oceaneng.2021.109048

[14] Ren, X. D., Tao, L. B., 2021. Nonlinear hydrodynamic characteristics of multi-body platform system. *European Journal of Mechanics - B/Fluids*. 89, 509-524. https://doi.org/10.1016/j.euromechflu.2021.06.008

[15] Hou, L., Wang, Q., 2022. Investigation about the hydrodynamic coupling characteristics of contra-rotating azimuth propulsor. *Brodogradnja*, 73(4), 79–105. https://doi.org/10.21278/brod73405

[16] Ardavanis, K., Nabergoj, R., Mauro, F., 2022. DP challenges in Ana platform jacket installation. *Brodogradnja*, 73(4), 1–11. https://doi.org/10.21278/brod73401

[17] Zhao, S., Gao, Z., Meng, X., Li, H., 2023. Multibody coupled dynamic response analysis of a dual barge float-over operation system with motion compensation equipment under a passive operational mode, *Ocean Engineering*, 269, 113499. https://doi.org/10.1016/j.oceaneng.2022.113499

[18] Chen, M., Ouyang, M., Li, T., Zou, M., Ye, J., Tian, X., 2023. Numerical modelling of a catamaran float-over deck installation for a spar platform with complex hydrodynamic interactions and mechanical couplings, *Ocean Engineering* , 287, 115905. https://doi.org/10.1016/j.oceaneng.2023.115905

[19] Ji, M. Y., Sharath S., Yasunori N., 2023. Characteristic of hydrodynamic derivatives for a multi-hull navigation vessel in dynamic positioning mode. *Ocean Engineering*, 278,114271. https://doi.org/10.1016/j.oceaneng.2023.114271

[20] Zou, M. Y., Chen, M. S., Zhu, L., Li, L., Zhao, W. H., 2023. A constant parameter time domain model for dynamic modelling of multi-body system with strong hydrodynamic interactions, *Ocean Engineering*, 268, 113376. https://doi.org/10.1016/j.oceaneng.2022.113376

[21] Ren, H. L., Wang, X. L., Hu, Y. J., Li, C.G., 2007. Dynamic Response Simulation of Lifting Load System of Ship-mounted Cranes. *Journal of System Simulation*, 19(5), 2665–2668. (in Chinese)

[22] Yang, B. L., 2008. Research on Dynamic Simulation of the Deck Crane Structure Based on Virtual Prototype Technology. Wuhan University of Technology.

[23] Wang, X. L., You, X. Y., Hu, Y. J., 2010. Cargo Pendulation Analysis of Moored Crane Ship under Regular Waves. *China Mechanical Engineering*, 21, 1077–1082 (in Chinese).

[24] Zou, Y., 2012. Numerical Analysis of the Large Marine Crane Dynamic Response. Master's thesis, Liaoning: Dalian University of Technology.

[25] Lin, B. H., 2016. Research on Dynamic Analysis and anti-swing control of the Marine Crane Lifting System. Master's thesis, Liaoning: Dalian Marine University.

[26] Li, B., Huang, W., Chen, X., 2018. A numerical study of dynamic response of crane semi-submersible along TLP in tender-assisted drilling operation. *Ships and Offshore Structures*, 13 (sup1), 273-286. https://doi.org/10.1080/17445302.2018.1446707

[27] Lu, H.W., 2019. Model test study on motion response of large crane ship hoisting operation. *Chemical Industry Management*, 8, 152–153 (in Chinese).

[28] Milana, G., Banisoleiman, K., González, A., 2021. An Investigation into the Moving Load Problem for the Lifting Boom of a Ship Unloader. *Engineering Structures*, 234, 111899. https://doi.org/10.1016/j.engstruct.2021.111899

[29] Bozkurt, B., Melek E., 2023. Heave and Horizontal Displacement and Anti-Sway Control of Payload during Ship-to-Ship Load Transfer with an Offshore Crane on Very Rough Sea Conditions. *Ocean Engineering*, 267, 113309. https://doi.org/10.1016/j.oceaneng.2022.113309

[30] Sun, M.K., Wang, S. H., Han, G. D., Jin, G. L., Li, J., Chen, H. Q., Sun, Y. Q., 2023. Multi-Cable Anti-Swing System for Cranes Subject to Ship Excitation and Wind Disturbance: Dynamic Analysis and Application in Engineering. *Ocean Engineering*, 281, 114518. https://doi.org/10.1016/j.oceaneng.2023.114518

[31] Makarov, O., Takashi H., 2023. Parametric Sensitivity of Crane Ship Numerical Model with Experimental Verification in a Wave Basin. *Ocean Engineering*, 286, 115554. https://doi.org/10.1016/j.oceaneng.2023.115554

[32] Sano, M., 2023. Mathematical model and simulation of cooperative manoeuvres among a ship and tugboats. *Brodogradnja*, 74(2), 127–148. https://doi.org/10.21278/brod74207

[33] DNV, 2019. Rules for classification of Ships.

[34] International Maritime Organization, 2015. Fire Safety System Code (FSS Code).

[35] Marintek, 2012. SIMO—Theory Manual Version 4.0. Trondheim, Norway.

[36] CCS. 2020. Guidelines for Analysis of Transportation and Floatover of Large Offshore Structures.